Journal of Alloys and Compounds 536 (2012) 138–144

Contents lists available at SciVerse ScienceDirect

Journal of Alloys and Compounds

journal homepage: www.elsevier.com/locate/jalcom

Structural, electrical transport and NO_2 sensing properties of Y-doped ZnO thin films

Necmettin Kılınç [a,*], Sadullah Öztürk [a], Lütfi Arda [b], Ahmet Altındal [c], Zafer Ziya Öztürk [a,d]

[a] Gebze Institute of Technology, Science Faculty, Department of Physics, 41400 Gebze-Kocaeli, Turkey
[b] Bahçeşehir University, Faculty of Arts & Science, Besiktas Campus, 34349 Besiktas-Istanbul, Turkey
[c] Yıldız Technical University, Faculty of Arts & Science, Department of Physics, 34210 Davutpasa-Istanbul, Turkey
[d] TUBITAK Marmara Research Center, Institute of Material Science, 41470 Gebze Kocaeli, Turkey

ARTICLE INFO

Article history:
Received 13 April 2012
Received in revised form 22 April 2012
Accepted 24 April 2012
Available online 5 May 2012

Keywords:
Yttrium doped ZnO
CBH
VRH
NO_2 sensing
Conduction mechanism
Dip coating

ABSTRACT

Yttrium (Y) doped ZnO thin films with concentrations of 1 at.%, 5 at.% and 10 at.% Y concentrations were deposited on glass substrates by using sol–gel dip coating method. The electrical properties of the films were measured dependence on temperature to identify the dominant conduction mechanism. It was found that thermally activated band conduction was the dominant conduction mechanism at high temperatures whereas, in the low temperature region, the dependence of the dc conductivity on temperature followed Mott's variable range hopping (VRH) model. The temperature dependence of both the ac conductivity and the frequency exponent are reasonably well interpreted by the correlated barrier hopping (CBH) model. The imaginary part of the impedance at different temperatures shows a relaxation peak and its position shifts to higher frequency with increasing temperature. This suggests a temperature-dependent relaxation. As an application, the NO_2 sensing properties of the films were investigated at 200 °C in the concentration ranges of 100 ppb–1 ppm. The response characteristics of Y-doped ZnO films have shown a high sensitivity to NO_2 at this temperature and the highest sensor response were observed for 1 at.% Y-doped ZnO film.

© 2012 Elsevier B.V. All rights reserved.

1. Introduction

Due to their outstanding physical properties, such as high transparency, piezoelectricity, wide-band gap semiconductivity, room-temperature ferromagnetism, and magneto-optic effect, zinc oxide (ZnO) is considered to be among the promising materials for use in modern devices such as spin-polarized solar cells, magneto optical switches, gas sensors, optical waveguide, flat panel displays and transparent heat mirrors [1–5]. Numerous ZnO film preparation methods have been reported including r.f. and magnetron sputtering [6,7], chemical vapor deposition (CVD) [8] and sol–gel processes [9]. Among these methods, the sol–gel technique has made possible the fabrication of ZnO films with reproducible and desired properties. It is known that the physical properties of the ZnO material strongly depend on the deposition method. Ogawa et al. [10] and Natsume et al. [11] reported that generally the resistivity of the films prepared by sol–gel method is sufficiently low relative to those prepared by other chemical methods like chemical vapor deposition. The application of the ZnO material for the above devices is related to the transport mechanism of charge carriers in this material. The use of dopants to improve the physical characteristics of technological materials such as ZnO, is widely implemented in both the commercial and research fields. Many researchers have reported that small concentrations of dopant material such as Al, Ga, Mg, Cu, and In can significantly affect the electrical and optical properties of ZnO [12–15]. Consequently, an accurate knowledge of the charge transport mechanism is critical if the ZnO is to be incorporated into the family of materials considered for designing devices. Although extensive studies have been performed on the dc electrical properties of ZnO with various doping in recent years, it seems that research on the ac electrical behavior of ZnO thin films, especially the yttrium (Y) doped ZnO, has been insufficient.

In this article we focused on the deposition of Y-doped ZnO films using dip coating technique of sol–gel process. The temperature dependence of both dc and ac electrical conductivity of the ZnO films with different Y doping concentrations is assessed in temperature range of 300–473 K to determine the carrier transport mechanism in the films. The frequency and the temperature-dependent impedance measurements and NO_2 gas sensing properties at 200 °C of ZnO and Y-doped ZnO films were also investigated.

2. Experimental

All the starting materials were analytical grade and were used without further purification. Yttrium (Y) doped zinc oxide (ZnO) films were prepared on glass substrate by repeated dip-coating. Zinc acetate dihydrate ($C_4H_6O_4Zn{\cdot}2H_2O$) and

* Corresponding author. Address: Department of Physics, Science Faculty, Gebze Institute of Technology, P.O. Box 141, 41400 Gebze-Kocaeli, Turkey. Tel.: +90 2626051312; fax: +90 262 6538490.
E-mail address: nkilinc@gyte.edu.tr (N. Kılınç).

0925-8388/$ - see front matter © 2012 Elsevier B.V. All rights reserved.
http://dx.doi.org/10.1016/j.jallcom.2012.04.104

Yttrium acetate ($Y(OOCCH_3)_3{\cdot}4H_2O$) were used as Zn and Y sources, respectively. Coating solution was prepared by dissolving zinc acetate dihydrate in methanol and acetyl acetone, a well known sol stabilizer reagent. The molarity of the zinc acetate was chosen to be 0.025 M. Y doping was achieved by adding calculated amounts of yttrium acetate to the precursor solution and its concentration was adjusted from 1 to 10% mol in the present work. 1 at.%, 5 at.%, 10 at.% Y-doped ZnO and undoped ZnO samples were designated as abbreviations of **B1**, **B2**, **B3** and **B4**, respectively. In order to obtain a clear and homogenous solution to serve as precursor, the resultant mixture solution was stirred at room temperature for 8 h. For improving the adhesion of the film on glass substrates, triethanolamine was added to the precursor solution. The glass substrates, after cleaning with acetone, methanol and deionized water in an ultrasonic bath for 10 min each, were dipped in the solution each, withdrawn at a rate of 0.2 m/min. After dipping in solution, the samples were pre-annealed at 300 °C for 5 min. This cycle was repeated 3 times. The thickness of the films was in the range of 70–100 nm. The deposited films were annealed in air at 600 °C for 30 min.

The structural properties of the films were investigated by Rigaku X-ray diffractometer (D/MAX 2200) with CuK_α as the source of radiation at 40 kV and 40 mA in the scanning angle of 10–70°. The surface morphology of the films was analyzed by scanning electron microscopy (SEM, JEOL 5910LV). Energy Dispersive X-ray spectroscopy (EDX) studies have been carried out to confirm the composition of the films.

For electrical and gas sensing measurements, gold electrodes with a thickness of about 50 nm in rectangular form separated by 1 mm were thermally evaporated on Y-doped ZnO films at pressure 5×10^{-6} mbar in thermal evaporation system (Leybold Univex 450). The dc and ac electrical conductivity measurements were performed under N_2 flow (flow rate: 200 sccm) in the temperature range of 300–473 K. The current–voltage (I–V) measurement was carried out with a Keithley 6517A Electrometer/High Resistance Meter. Impedance measurements were ascertained with a Hewlett–Packard 4294A impedance analyzer in the frequency range 40 Hz–1 MHz. The effect of the NO_2 gas on the resistance of the films was measured in a homemade chamber with volume of 1 L. Nitrogen was used as carrier gas in the experiments with a purity level of 99.999%. Diluted NO_2 gas (1%) in high purity N_2 was used as target gas. First, the test chamber was purged with high purity N_2 flow (flow rate: 200 sccm) until the resistance reached a steady value and then the chamber was closed. Then diluted NO_2 gas in high purity N_2 was injected with a gastight micro syringe to reach the concentration of 100 ppb (10 μl), and the resistance was recorded during a period of time necessary to calculate the response time of the sensor and then, the test chamber was opened and was cleaned with high purity N_2 flow for recovery. The procedure was repeated for all concentration levels. The resistance was monitored continuously and recorded using an IEEE 488 data acquisition system incorporated to a personal computer during the measurements.

3. Results and discussion

3.1. Structural characterization

Y-doped ZnO thin films were coated on glass substrate using the reel-to-reel sol–gel coating system. Nano powders and the thin films were annealed at 600 °C for 30 min under air using box furnace. The quality of thin film depends on the withdrawal rate, the drying process, the heat treatment conditions and the sol structure such as the chemical composition, the purity of precursor solvent catalyst materials and the pH value of starting and stabilized solution.

XRD analysis was used to find phase and crystal structure of the Y-doped ZnO nano powders prepared under the same conditions. The X-ray diffractions of the Y-doped ZnO nano powders with various at.% ratios are shown in Fig. 1. For ZnO and 1 at.% Y-doped ZnO, all the peaks belong to the hexagonal lattice of ZnO, and no indications of a secondary phase were found. But, two phases ZnO and Y_2O_3 were identified in the diffraction patterns for 5 at.% Y-doped ZnO (**B2**). Similarly, both phases ZnO and Y_2O_3 were identified in the diffraction patterns for 10 at.% Y-doped ZnO (**B3**). In addition, the EDX spectrums of the **B1**–**B3** Y-doped ZnO thin films showed that Zn, Y, O and Si peaks were observed for 5 at.% (**B2**) and 10 at.% (**B3**) Y-doped ZnO thin films, but Y peak was not clear for 1 at.% (**B1**) Y-doped ZnO thin film. Si peak in EDX spectrum came from glass substrate.

Fig. 2 depicts surface morphologies of 1, 5 and 10 at.% Y-doped ZnO thin films (**B1**–**B3**). Surface of thin films are dense, however some parts of thin films are observed variety of homogeneity, pinhole and porosity. The all SEM images are in same magnification. It

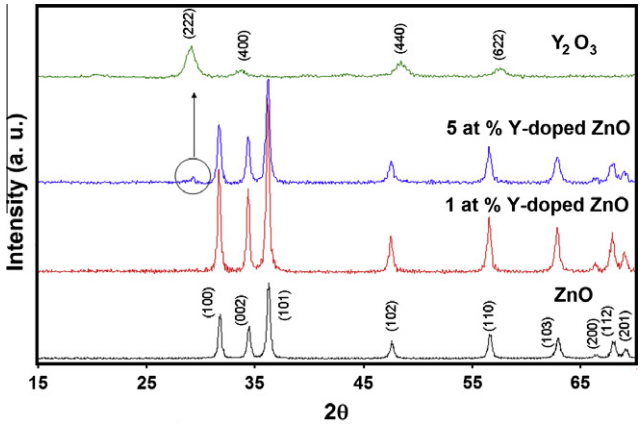

Fig. 1. X-ray diffraction of undoped and Y-doped ZnO nano powders at different dopant concentrations.

is clearly seen from Fig. 2 that the grain size of the thin films is decreased with increasing doping concentration. The grain sizes are approximately 40 nm (Fig. 2a), 30 nm (Fig. 2b) and 20 nm (Fig. 2c) for 1, 5 and 10 at.% Y-doped ZnO thin films, respectively.

3.2. Electrical conductivity analysis

3.2.1. Dc conductivity

The ZnO thin films with varying Y doping concentration have been deposited on glass substrates by using sol–gel method. The electrical conductivity of Y doped samples was studied from room temperature to 473 K. Fig. 3 shows the dc conductivity of Y doped ZnO films as a function of Y concentration at room temperature. It is clearly seen from the figure that the conductivity of Y doped ZnO film is higher than that of undoped ZnO thin film. On the other hand, the conductivity of doped films decreased with increasing doping concentration (Fig. 3). Similar results have been observed in gallium doped ZnO thin film [16], Yttrium doped sol–gel ZnO thin film [17], dc magnetron sputtered Al doped ZnO thin film [2] and fluorine doped ZnO thin film [18].

It is known that the intrinsic defects generated at high temperature and the dopants, whether specifically added to the material or not, are the most important two factors that control the electrical conductivity of ZnO. The overall variation in dc conductivity with Y doping can be explained as follows: when a small amount of Y introduced it ionizes as a Y^{3+} and can easily be substituted for Zn^{2+} site without pronounced lattice distortion. This substitution generates an extra free electron in conduction band thereby increasing electrical conductivity. By increasing the doping concentration further, the conductivity decreases because of grain boundary scattering of the carriers and segregation of Y at the grain boundaries. It is clearly seen from SEM image of 1, 5 and 10 at.% Y-doped ZnO thin films (Fig. 2) the grain size is decreased. Hence, the decrease in the conductivity is related to grain boundary density at the surface.

The temperature dependence of the measured conductivity of all the samples prepared at the same conditions and having different doping concentration of Y is presented in Fig. 4a. From which it is apparent that the conductivity of the films increases with the increase in temperature showing semiconducting behavior. The general behavior of the conductivity curves can be read as the presence a clear deviation from the Arrhenius law. A relatively weak temperature dependence of the conductivity in low temperature region and strong temperature dependence at higher temperature region can be distinguished easily for all samples.

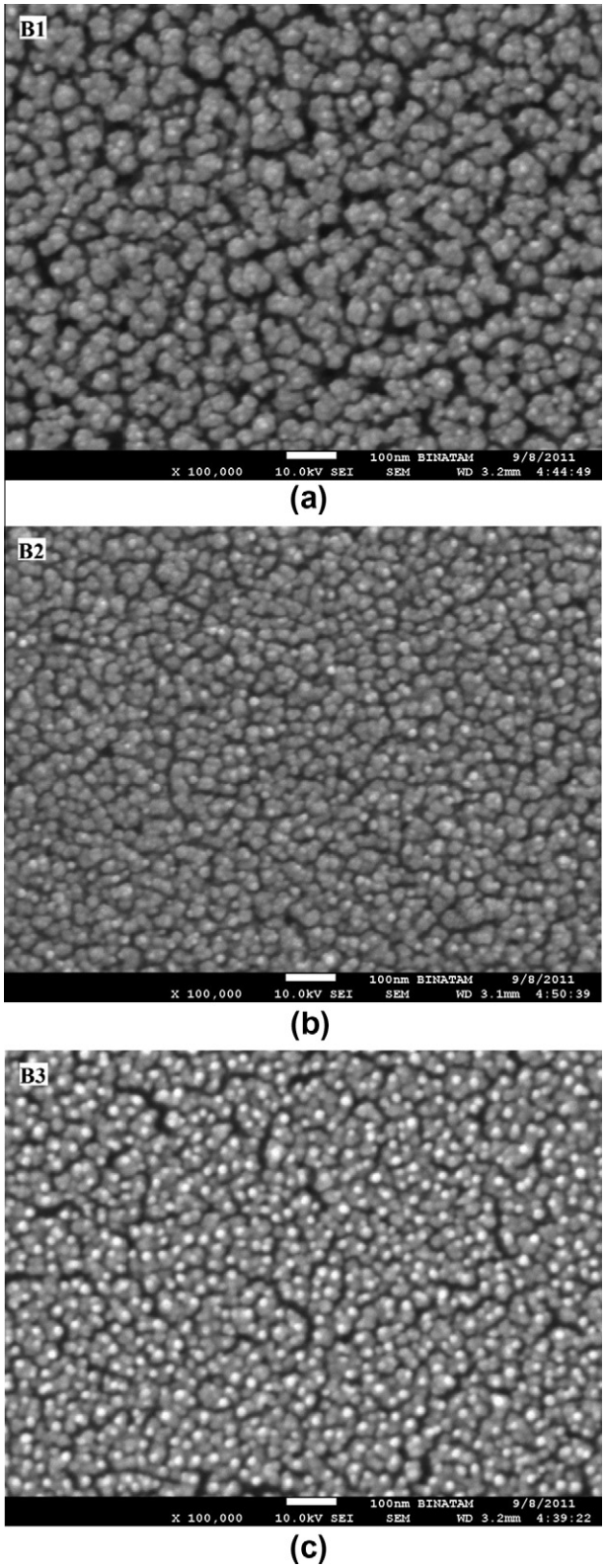

Fig. 2. The SEM morphologies of Y-doped ZnO samples **B1** (a), **B2** (b) and **B3** (c).

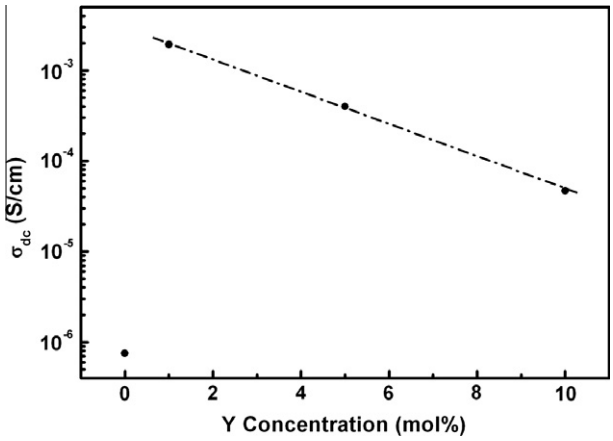

Fig. 3. Dc conductivity of the Y-doped ZnO films as a function of Y concentration at room temperature.

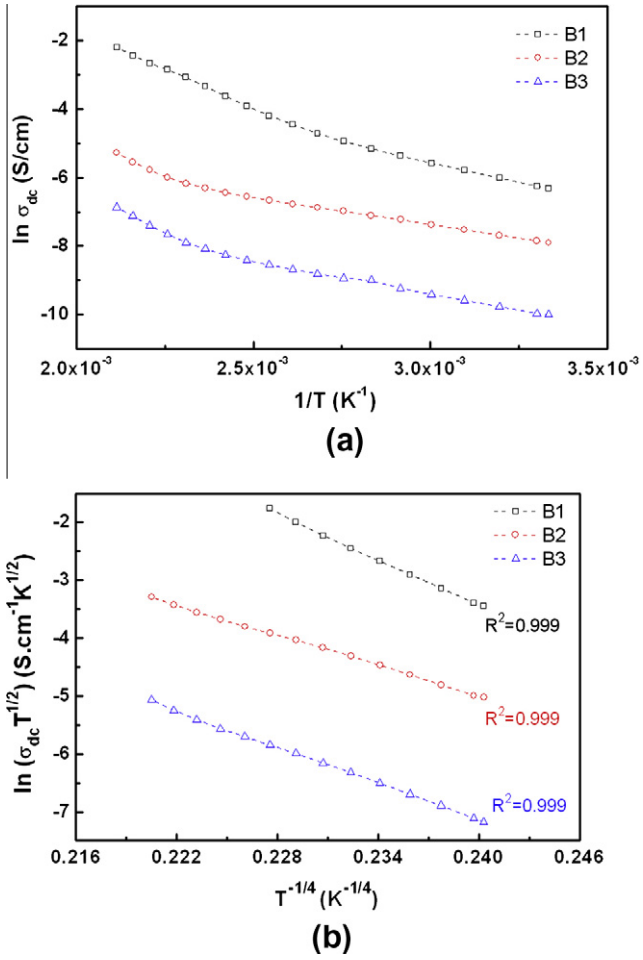

Fig. 4. Variation of dc electrical conductivity with temperature (a), and plot of ln ($\sigma_{dc}T^{1/2}$) versus $T^{-1/4}$ in the low temperature region (b) for all Y-doped ZnO samples.

As can be seen from Fig. 4a, a good linear dependence having a linearity factor better than 0.99 in high temperature region shows that the thermally activated type of conduction is dominating. In this case the temperature dependence of the conductivity can be expressed as,

$$\sigma_{dc}(T) = \sigma_0 \exp\left(-\frac{E_A}{kT}\right) \quad (1)$$

where E_A is the activation energy, T is the temperature, k is the Boltzmann constant and σ_0 is the constant of proportionality. With the aid of Eq. (1), the values of the activation energies were calculated from the slopes of Fig. 4a which give, E_A = 0.39, 0.36 and

0.43 eV for **B1**, **B2** and **B3**, respectively. These values of E_A are in agreement with the reported values of E_A for doped ZnO [19].

On the other hand, weak temperature dependence of dc conductivity in low temperature region indicates that the thermally activated type conduction is not a dominating conduction mechanism in any more. At low temperatures, the experimentally obtained data can be analyzed using variable range hopping (VRH) model proposed by Mott [20]. VRH model is used to justify the charge transport mechanism by localized energy states. Localized states can be produced due to several reasons such as, distorted bond angles, defect centers and impurities either of which can yield localized states. In general, these localized states are close in energy levels, therefore, only small activation energy is required for the processing of hopping process and the hopping can occur at low temperatures. The Mott relation for conductivity of a semiconductor is given by:

$$\sigma_{dc}\sqrt{T} = \sigma_{0h}\exp\left(-\left(\frac{T_0}{T}\right)\right)^{\frac{1}{4}} \quad (2)$$

where σ_{0h} and T_0 are given by the following equations

$$\sigma_{0h} = 3e^2\upsilon_{ph}\left(\frac{N(E_F)}{8\pi\alpha k}\right)^{\frac{1}{2}} \quad (3)$$

$$T_0 = \frac{\lambda\alpha^3}{kN(E_F)} \quad (4)$$

where υ_{ph} is the phonon frequency at Debye temperature, α is the inverse localization length of wave function for localized state, $N(E_F)$ is the localized state density for electrons at Fermi level and $\lambda = 16$. In order to check the applicability of VRH model in Y-doped ZnO films at low temperatures, the plot of ln $(\sigma_{dc}T^{1/2})$ versus $T^{-1/4}$ has been shown in Fig. 4b. As can be seen from Fig. 4b, a linear variation in conductivity with $T^{-1/4}$ (having a linearity factor better than 0.99) was observed for all Y-doped ZnO samples, indicating the origin of dc conduction mechanism as variable range hopping at low temperature. Several research groups have reported such a linear dependence of conductivity in accordance with VRH model in low temperatures for the films of doped ZnO [21–23]. The values the characteristic temperature T_0 were calculated from slopes of the fitted lines. The VRH results are listed in Table 1. The VRH model gives two other hopping parameters that are the most probable hopping jump distance R and the average hopping energy W. To be making sure from the validity of VRH model in Y-doped ZnO thin films, we calculated R and W values by using the following expressions [24].

$$R = \left(\frac{9}{8\pi kTN(E_F)}\right)^{\frac{1}{4}} \quad (5)$$

$$W = \frac{3}{4\pi R^3 N(E_F)} \quad (6)$$

For the VRH conduction process, it is required that $\alpha R > 1$ and $W > kT$. In the present case it may be noted from Table 1 that the conditions $\alpha R > 1$ and $W > kT$ are satisfied for all compositions of Y-doped ZnO films and justifying the applicability VRH conduction model in low temperature region.

3.2.2. Ac conductivity

To differentiate as well as to identify the origin of the charge transport mechanism, the ac response of Y-doped ZnO thin films to a sinusoidal stimulus are investigated. Fig. 5 shows the frequency dependence of ac electrical conductivity of **B1** at different fixed temperatures on a logarithmic scale. It is clear that, the plot of ln $(\sigma_{ac}(\omega,T))$ versus ln (ω) emphasizes generally two regions; a frequency independent response at low frequencies and a crossover to a linear increase with frequency. Similar frequency dependency was observed for other samples. At moderately high frequencies, the linear dependence for logarithm of ac conductivity on logarithm of frequency implies [25].

$$\sigma_{ac}(\omega,T) = A\omega^s \quad (7)$$

where A is a constant depending on temperature, ω is the angular frequency of applied signals and s is an exponent whose value and behavior with respect to temperature determine the dominant conduction mechanism in the samples.

The frequency exponent s is calculated from the slope of ln $(\sigma_{ac}(\omega,T))$ versus ln (ω) graph. Fig. 6 shows the variation of exponent s with temperature for all Y-doped ZnO thin films. Several models have been developed to explain the temperature dependence of ac conductivity and exponent s. In quantum mechanical tunneling (QMT) model which is based on the tunneling of an electron through a barrier separating two localized states near the Fermi level [26], the exponent s is temperature independent and has a value of 0.8. As can be discerned from Fig. 6, the exponent is found to decrease with increasing temperature for all samples investigated in contrast to the QMT model. Small polaron tunneling (SPT) [27] model is also not a suitable mechanism for explaining the results of our investigations because SPT model predicts an increase of exponent with the increase of temperature, in sharp contrast with our observations as delineated in Fig. 6. Large polaron tunneling (LPT) model predicts a minimum in the temperature dependence of exponent [28], which is not observed in our results. Therefore, LPT model is also not applicable for the present films. The correlated barrier hopping (CBH) model which is developed by Elliot [25], describes charge carriers hopping among sites over the potential barrier separating them rather than tunneling through the barrier.

In CBH model a temperature dependent exponent is predicted, with exponent decreasing as the temperature increases and exponent increasing towards unity as the temperature tends to zero, in contrast to QMT model. The temperature dependence of s (Fig. 6), is consistent with the prediction of CBH model. Additionally, CBH model predicts a linear dependence of ac conductivity on temperature. The ac conductivity is increased with increasing temperature for the sample of **B1** as shown in Fig. 5. In order to check the applicability of CBH model, it was drawn ac conductivity versus temperature graph at the fixed frequencies for all Y doped ZnO thin film samples. It is observed that, ac conductivity increases linearly with the increase of temperature and the linearity factor is better than 0.99 for all samples. These results reveal that CBH model is a suitable model for the charge transport in Y-doped ZnO thin films. In summary, our ac analysis based on the existing theories showed that, we have no results supporting QMT, SPT and LPT models. On the other hand, we found that both the temperature depen-

Table 1
Mott parameters for Y-doped ZnO thin films.

Sample	T_0 (K)	N (cm^{-3}/eV)	α (cm^{-1})	R (cm)	W (eV)	αR
B1	3.0×10^8	1.7×10^{17}	6.5×10^6	1.9×10^{-6}	0.21	12.4
B2	5.7×10^7	1.3×10^{17}	1.6×10^6	5.1×10^{-6}	0.14	8.2
B3	1.2×10^8	2.6×10^{17}	2.6×10^6	3.7×10^{-6}	0.17	9.6

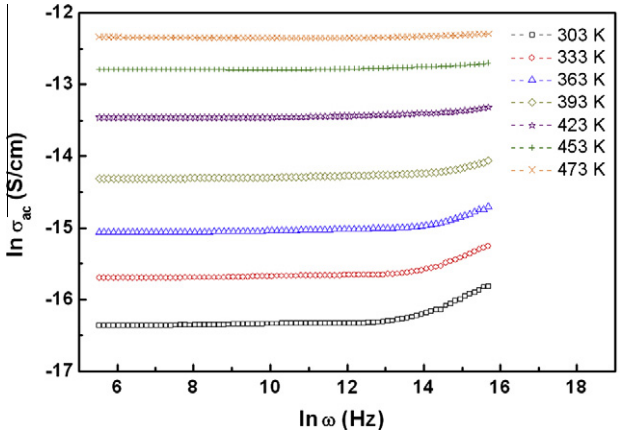

Fig. 5. Frequency dependence of ac conductivity of a typical Y-doped ZnO thin film (**B1**) at indicated temperatures.

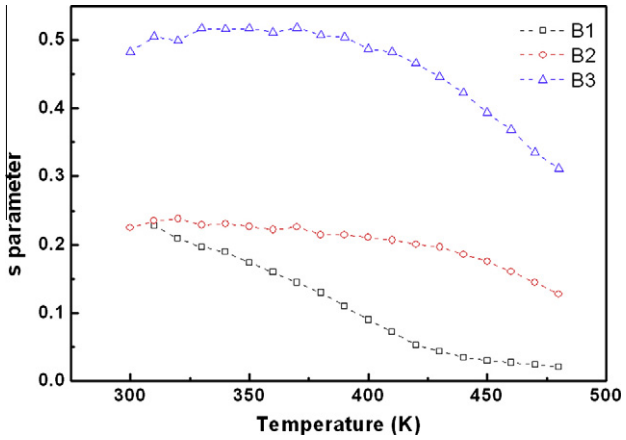

Fig. 6. Variation of frequency exponent *s* with temperature for all Y-doped ZnO samples.

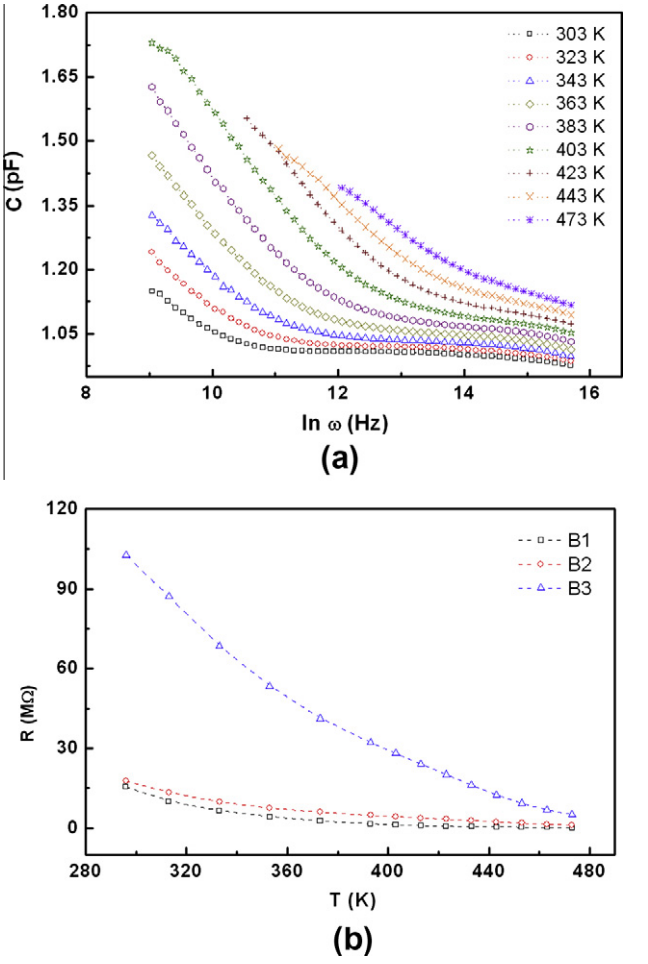

Fig. 7. Frequency dependence of ac capacitance for the sample of **B1** at different temperatures (a) and variation of resistance with temperature at 1 kHz fixed frequency for all samples (b).

dence of the exponent and ac conductivity is in good agreement with the CBH model for all samples.

3.2.3. Ac capacitance

Fig. 7a depicts the variation of capacitance as a function of frequency at indicated temperatures for the sample of **B1**. Capacitance measurements demonstrated that the capacitance initially decreases rapidly with increasing frequency and subsequently approaches the low temperature values at higher frequencies. It is also clear from Fig. 7a that at low frequencies, the capacitance is strongly temperature dependent and that at high frequencies; the temperature dependence is weak. The frequency and temperature dependence of capacitance can be expressed by an equivalent circuit model which consists of a frequency independent capacitive element (C_1) in parallel with a temperature dependent resistive element (R_1), both in series with a resistance (R_2). In this case, the measured capacitance can be expressed as,

$$C = C_1 + \frac{1}{\omega^2 R_1^2 C_1^2} \tag{8}$$

It is expected that the measured capacitance C should decrease with increasing frequency at all temperatures in accordance with Eq. (8). As a representative result, the variation of resistance with temperature for 1 kHz fixed frequency for all samples is plotted in Fig. 7b. It is clear that the magnitude of the resistivity decreases with increasing temperature. Similar frequency and temperature dependence of capacitance have been observed in several inorganic materials such as magnetron sputtered titanium dioxide (TiO_2) thin films and ZnO pellets [29,30] and in some organic compounds like phthalocyanine thin films [31].

3.2.4. Impedance analysis

The dielectric properties of materials as a function of frequency can be normally described in terms of complex impedance (Z^*) which is defined as $Z^* = R - jX$, where R and X are real and imaginary part of complex impedance, respectively. To further elucidate our results based on the ac transport characteristics, impedance spectra of the samples was taken as function of temperature in the frequency range of 40 Hz–1 MHz. The main advantage of this technique is that the contributions of the bulk materials, the grain boundaries and electrode effects can be easily separated if the time constants are sufficiently different to allow separation [32]. The ac responses of the doped films have been investigated by the measurements of impedance spectra (capacitance, real and imaginary part of complex impedance) over the temperature range of 300–473 K.

The real (R) part of impedance for **B1** as function of frequency at various temperatures is shown in Fig. 8a. The effect of the temperature on the magnitude of R is clear especially at low frequency range. At low frequencies, the real part of the impedance shows a frequency independent region extending from dc to some characteristic frequency and then it becomes strongly frequency depen-

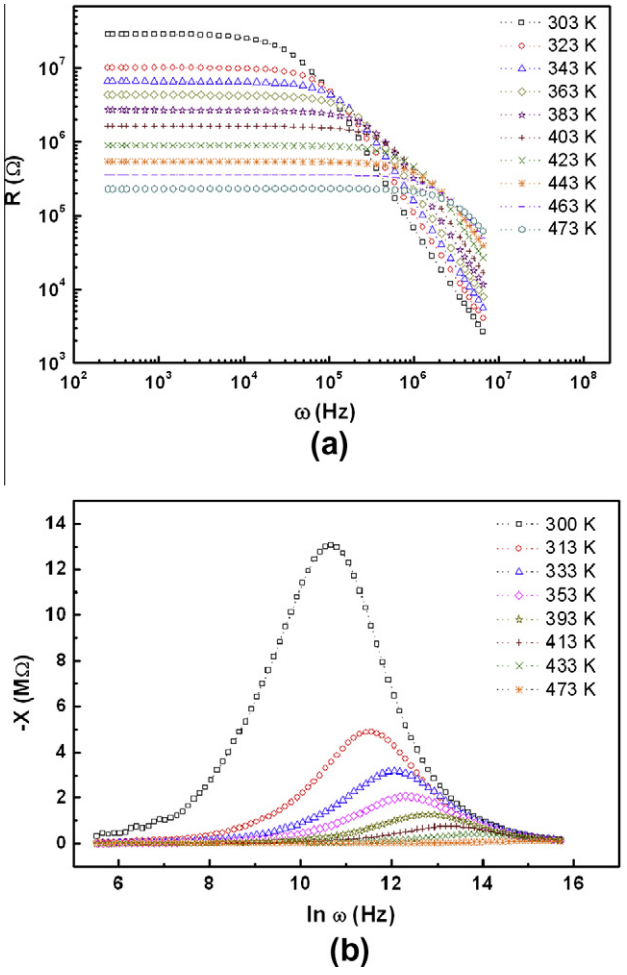

Fig. 8. Frequency dependence of real part of impedance at various temperatures (a) and frequency dependence of loss spectrum at indicated temperatures (b) for the sample of **B1**.

dent, decreasing rapidly with increasing frequencies. It is noticed that the transition frequency from the frequency independent region to frequency dependent region shifts to higher frequency with increasing temperature. The decrease in the real part of the impedance with frequency is in agreement with reported results in the literature [33].

The frequency dependence of loss spectrum, variation of the imaginary part of the complex impedance, of the same sample (**B1**) for different temperatures is shown in Fig. 8b. The obtained loss spectrum is characterized by few important features in the pattern such as (i) The loss spectrum at each temperature exhibits one relaxation peak (ii) The peak position shifts towards higher frequency with increasing temperature showing that the resistance of the bulk material is decreasing. The shift in the peak position is a further evidence of very broad distributions of relaxation times and there is apparently not a single relaxation time, and thereby relaxation process involved, but different relaxations with their own discrete relaxation times depending on the temperature. (iii) The magnitude of the imaginary part of impedance decreases with increasing temperature. At low temperatures, there is a typical peak broadening with increase in temperature and at high temperatures, the curves appear almost flat. This type of temperature dependence is attributed to the presence of a space charge in the material.

3.3. NO_2 gas sensing

The sensors were tested in resistive mode by measuring the resistance of the sensor with respect to time while charging the target gas i.e. NO_2 into the chamber. Fig. 9 illustrates how NO_2 gas in low concentrations in the test chamber produces a reversible increase in the resistance of **B1** at 473 K. After the resistance of the sample of **B1** was measured under N_2 flow for 20 min to obtain base line, the measurement chamber was closed and then, 100 ppb NO_2 was injected into the chamber. After the sample was exposed to100 ppb NO_2, the resistance of **B1** is increased from 10 MΩ to a maximum value of 22 MΩ in 30 s, then the resistance starts to decrease slowly (Fig. 9). When the sample was purged with N_2 flow, the resistance of the sample was decreased slowly to baseline for 10 min. Similar behavior was observed for exposure to second 100 ppb and the other concentrations of NO_2. Previously, we synthesized different nanostructured ZnO and investigated NO_2 sensing properties of them by using high purity N_2 as carrier gas and found high and rapid sensor response [34]. It is clear from Fig. 9 that the interaction of NO_2 with Y-doped ZnO film leads to a fast increase in its resistivity, which continues to rise until the NO_2 gas is turned off (typically after 1 min). The original resistivity is restored approximately 10 min, after the NO_2 flow is turned off and the measurement cell is purged with dry air. Similarly, the NO_2 sensing measurements for the two samples (**B2** and **B3**) were carried out and with comparable outcomes. The increase in resistivity of the sensor can be explained as follows. It is a well known fact that ZnO is an n-type semiconductor. It is also well established that electron donor or electron acceptor molecules can reduce or oxidize the ZnO. NO_2 is a well-known oxidizing gas which, on con-

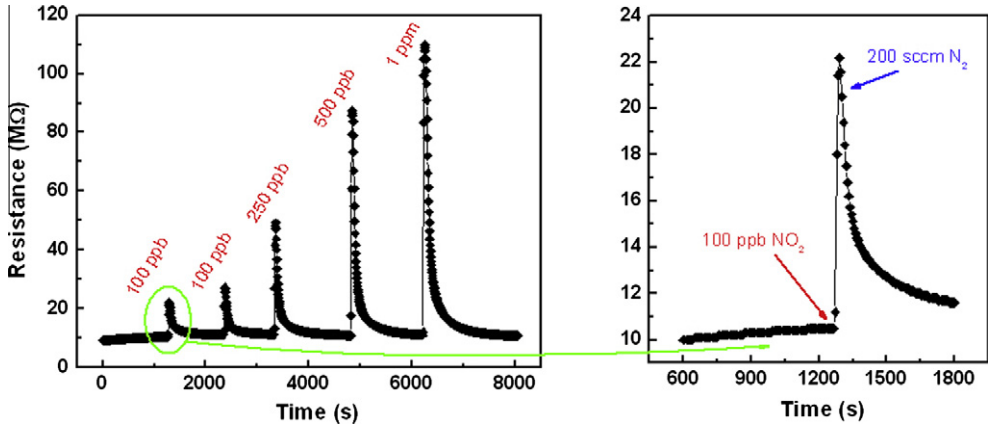

Fig. 9. The resistance versus time curves for the sample of **B1** exposed to the 100 ppb–1 ppm NO_2 in high-purity N_2 at 473 K.

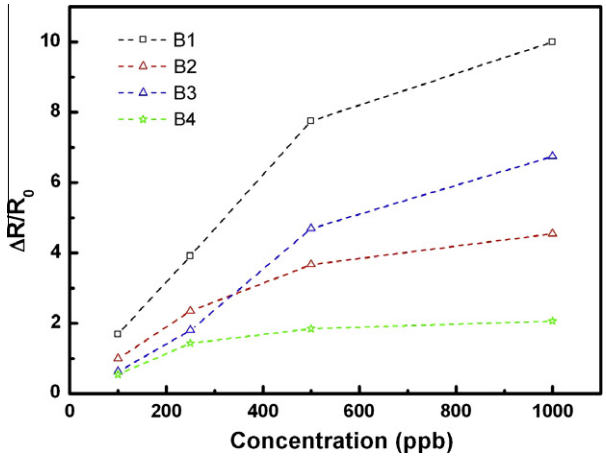

Fig. 10. The sensor response versus concentration graph for all samples (**B1**–**B4**) at 473 K.

tact with Y-doped ZnO film surface, causes the transfer of an electron from the ZnO to the NO_2 gas molecule. So, the resistance of ZnO increases with NO_2 adsorption. Consequently, the decrease in the n-type oxide film justifies the increased resistivity of the film. Adsorbed NO_2 acts as an acceptor in the oxide in accordance with the following reversible doping process:

$$NO_2\ (gas) \leftrightarrow NO_2\ (ads)$$
$$e^- + NO_2\ (ads) \leftrightarrow NO_2^-\ (ads)$$

In general, gas response of a sensor is defined as the ratio of change in the resistance for the sensitive layer while being exposed to the original resistance.

$$\text{Response} = \frac{\Delta R}{R_0} \tag{9}$$

where ΔR is the change in resistance and R_0 is the reference in the target gas. The dependence of sensor responses on NO_2 gas concentration is shown in Fig. 10 for 1, 5 and 10 at.% Y-doped and undoped ZnO thin films. As can be seen from Fig. 10 that, the doped films have higher sensor response than undoped film. It is also clear that maximum sensor response is observed for 1% mol Y doped ZnO sample (**B1**) in the all concentration range. Previously, few reports have been published about NO_2 sensing properties doped ZnO films or nanostructures [35–40]. They found that doped ZnO films or nanostructures shows higher responses than their undoped films or nanostructures.

4. Conclusions

1 at.%, 5 at.% and 10 at.% Y-doped and undoped ZnO thin films were deposited on glass substrates by the sol–gel dip coating method. The temperature dependent dc and ac electrical conductivity of Y-doped ZnO thin films were investigated over the temperature range of 300–473 K under high purity N_2. XRD studies showed that a single-phase compound was formed exhibiting hexagonal lattice of ZnO. The dc conductivities results indicated that the carrier transport mechanism is the variable range hopping at low temperatures and the thermally activated type conduction at high temperature region. The ac conductivity was found to follow the CBH model throughout the temperature range under consideration. Dependences of the ac capacitance on the frequency and the temperature were elucidated in accordance to the equivalent circuit model. The NO_2 gas sensing properties of Y-doped ZnO films were also examined. The results of the examination demonstrated that Y-doped ZnO films have considerable sensitivity, rapid response and recovery, to low concentration of NO_2 gas.

Acknowledgements

This study was partially supported by TUBITAK project entitled "Development of Automotive Gas Sensors Based on Nano-Metal-Oxide Semiconductor with increased Selectivity, Sensitivity and Stability" (Project No. 111M261) and by DPT project entitled "Nanomagnetism and Spintronics Research Center" (Project No. 2009K120730).

References

[1] R.P. Davies, C.R. Abernathy, S.J. Pearton, D.P. Norton, M.P. Ivill, F. Ren, Chemical Engineering Communications 196 (2009) 1030–1053.
[2] H.X. Liu, H. Qiu, X.B. Chen, M.P. Yu, M.W. Wang, Current Applied Physics 9 (2009) 1217–1222.
[3] K.R. Kittilstved, N.S. Norberg, D.R. Gamelin, Physical Review Letters 94 (2005) 147209.
[4] M.S. Park, B.I. Min, Physical Review B 68 (2003) 224436.
[5] Y. Shimizu, F.C. Lin, Y. Takao, M. Egashira, Journal of the American Ceramic Society 81 (1998) 1633–1643.
[6] J.B. Webb, D.F. Williams, M. Buchanan, Applied Physics Letters 39 (1981) 640–642.
[7] T. Hata, T. Minamikawa, O. Morimoto, T. Hada, Journal of Crystal Growth 47 (1979) 171–176.
[8] T. Schuler, M.A. Aegerter, Thin Solid Films 351 (1999) 125–131.
[9] W. Tang, D.C. Cameron, Thin Solid Films 238 (1994) 83–87.
[10] M.F. Ogawa, Y. Natsume, T. Hirayama, H. Sakata, Journal of Materials Science Letters 9 (1990) 1351–1353.
[11] Y. Natsume, H. Sakata, T. Hirayama, Physica Status Solidi A – Applied Research 148 (1995) 485–495.
[12] J.P. Han, P.Q. Mantas, A.M.R. Senos, Journal of the European Ceramic Society 21 (2001) 1883–1886.
[13] V. Fathollahi, M.M. Amini, Materials Letters 50 (2001) 235–239.
[14] G. Juarez-Diaz, J. Martinez, M.L. Garcia-Cruz, R. Pena-Siera, J.A. Garcia, M. Pacio, Physica Status Solidi (C) 7 (2010) 957–959.
[15] N. Kilinc, L. Arda, S. Ozturk, Z.Z. Ozturk, Crystal Research and Technology 45 (2010) 529–538.
[16] G.K. Paul, S.K. Sen, Materials Letters 57 (2002) 742–746.
[17] Q.J. Yu, H.B. Yang, W.Y. Fu, L.X. Chang, J. Xu, C.L. Yu, R.H. Wei, K. Du, H.Y. Zhu, M.H. Li, G.T. Zou, Thin Solid Films 515 (2007) 3840–3843.
[18] A. Sanchez-Juarez, A. Tiburcio-Silver, A. Ortiz, E.P. Zironi, J. Rickards, Thin Solid Films 333 (1998) 196–202.
[19] A. Sawalha, M. Abu-Abdeen, A. Sedky, Physica B – Condensed Matter 404 (2009) 1316–1320.
[20] N.F. Mott, E.A. Davis, Calendon Press, Oxford, 1979.
[21] R. Kumar, N. Khare, Thin Solid Films 516 (2008) 1302–1307.
[22] Y.J. Ma, Z. Zhang, F. Zhou, L. Lu, A.Z. Jin, C.Z. Gu, Nanotechnology 16 (2005) 746–749.
[23] S. Bandyopadhyay, G.K. Paul, R. Roy, S.K. Sen, S. Sen, Materials Chemistry and Physics 74 (2002) 83–91.
[24] N.F. Mott, Journal of Non-Crystalline Solids 1 (1968) 1–17.
[25] S.R. Elliott, Advances in Physics 36 (1987) 135–218.
[26] M. Pollak, Philosophical Magazine 23 (1971) 519.
[27] A.R. Long, Advances in Physics 31 (1982) 553–637.
[28] M. Pollak, G.E. Pike, Physical Review Letters 28 (1972) 1449.
[29] B. Karunagaran, S.J. Chung, E.K. Suh, D. Mangalaraj, Physica B – Condensed Matter 369 (2005) 129–134.
[30] P.P. Sahay, S. Tewari, R.K. Nath, S. Jha, M. Shamsuddin, Journal of Materials Science 43 (2008) 4534–4540.
[31] M. Canlica, A. Altindal, A.R. Ozkaya, B. Salih, O. Bekaroglu, Polyhedron 27 (2008) 1883–1890.
[32] E. Barsoukov, J.R. Macdonald (Eds.), Impedance Spectroscopy: Theory, Experiment, and Applications, Wiley-Interscience, New Jersey, 2005.
[33] R. Thangavel, V. Sabarinathan, S. Ramasamy, J. Kumar, Materials Letters 61 (2007) 4090–4093.
[34] S. Ozturk, N. Kilinc, N. Tasaltin, Z.Z. Ozturk, Thin Solid Films 520 (2011) 932–938.
[35] S.T. Shishiyanu, T.S. Shishiyanu, O.I. Lupan, Sensors and Actuators B – Chemical 107 (2005) 379–386.
[36] N. Koshizaki, T. Oyama, Sensors and Actuators B – Chemical 66 (2000) 119–121.
[37] C. Siriwong, K. Wetchakun, A. Wisitsoraat, S. Phanichphant, Sensors IEEE (2009) 118–123.
[38] R. Ferro, J.A. Rodriguez, P. Bertrand, Thin Solid Films 516 (2008) 2225–2230.
[39] S.L. Bai, L.Y. Chen, D.Q. Li, W.S. Yang, P.C. Yang, Z.Y. Liu, A.F. Chen, C.L. Chung, Sensors and Actuators B – Chemical 146 (2010) 129–137.
[40] O. Lupan, S. Shishiyanu, L. Chow, T. Shishiyanu, Thin Solid Films 516 (2008) 3338–3345.